Exciton Lifetime Tuning by Changing the Plasmon Field Orientation with Respect to the Exciton Transition Moment Direction: CdTe–Au Core–Shell Nanorods

ARTICLE *in* NANO LETTERS · MARCH 2009

Impact Factor: 13.59 · DOI: 10.1021/nl900183m · Source: PubMed

NANO LETTERS

2009
Vol. 9, No. 3
1242-1248

Exciton Lifetime Tuning by Changing the Plasmon Field Orientation with Respect to the Exciton Transition Moment Direction: CdTe-Au Core−Shell Nanorods

Svetlana Neretina, Wei Qian, Erik C. Dreaden, and Mostafa A. El-Sayed*

Laser Dynamics Laboratory, School of Chemistry and Biochemistry, Georgia Institute of Technology, Atlanta, Georgia 30332-0400

Robert A. Hughes,† John S. Preston,†,‡ and Peter Mascher‡

Brockhouse Institute for Materials Research, McMaster University, Hamilton, Ontario, L8S 4M1, Canada, and Department of Engineering Physics, McMaster University, Hamilton, Ontario, L8S 4L7, Canada

Received January 19, 2009

ABSTRACT

We studied the anisotropy of the influence of plasmonic fields, arising from the optical excitation of a gold nanoshell plasmon absorption at 770 nm, on the lifetime of the bandgap state of the CdTe core in vertically aligned CdTe-Au core−shell nanorods. The previously observed decrease in the lifetime was studied as a function of the tilt angle between the long axis of the nanorod and the electric field polarization direction of the plasmon inducing exciting light. It is observed that the strongest enhancement to the exciton relaxation rate occurs when the two axes are parallel to one another. These results are discussed in terms of the coupling between the exciton transition moment of the CdTe rod and the electric field polarization direction of the gold nanoshell plasmon at 770 nm, which was determined from theoretical modeling based on the discrete dipole approximation.

As fabrication processes for nanomaterials become more advanced, increasingly sophisticated nanostructures and ensembles of nanostructures become possible. These advancements will inevitably give rise to phenomena associated with dissimilar nanomaterials interacting with each other. Plasmonic materials, most notably silver and gold nanoparticles, provide an obvious opportunity in this regard. Photons in resonance with such structures become confined in a manner which leads to the coherent oscillation of conduction band electrons. The oscillations inevitably give rise to electric fields which are known to be quite strong and extend well beyond the spatial extent of the nanostructure. Intriguing is the prospect of exciting these surface fields with resonantly coupled light so as to induce a separate response in a second material in close proximity. Already there exists a multitude of demonstrations where plasmonic materials have been used in this manner. The most well-known example is surface enhanced Raman scattering (SERS) where the detectability of molecules is increased by many orders of magnitude when adsorbed on a nanotextured gold or silver surface.[1,2] Recent reports of solar cell efficiencies being positively influenced by the placement of plasmonic particles on the active surface of the cell provide another intriguing demonstration.[3−6] The interaction between plasmonic and semiconducting nanostructures has proved especially rewarding. Lee et al.[7] performed an experiment using CdTe nanowires, where they observed a quenching of the photoluminescence when the nanowire was covered with a shell of gold. However, by simply separating the nanowire from the gold nanoshell with a 5 nm thick layer of protein molecules, they were able to observe a 5-fold increase in the emission quantum yield from the nanowires. This dramatic reversal in the response was attributed to the fact that the intermediate layer was thick enough to severely limit the efficient electron and energy transfer processes, but thin enough to be within the surface plasmon-exciton coupling range. In a follow-up publication,[8]

* To whom correspondence should be addressed. E-mail: melsayed@gatech.edu. Telephone: 404-894-0292.
† Brockhouse Institute for Materials Research.
‡ Department of Engineering Physics.

10.1021/nl900183m CCC: $40.75
Published on Web 02/23/2009

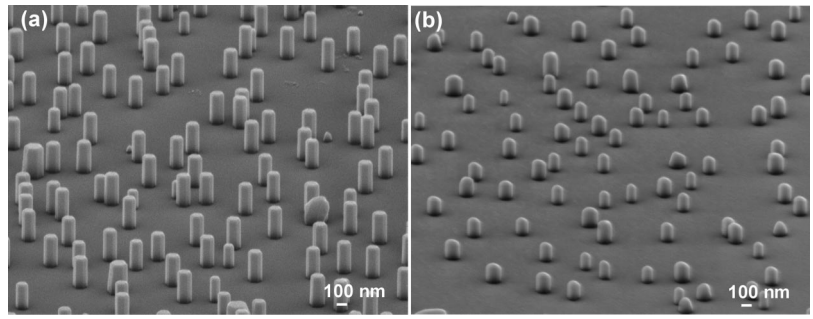

Figure 1. SEM images of CdTe-Au core−shell nanorods with aspect ratios (a) ≥3 and (b) ≤2. Typical core−shell nanorod heights for the low and high aspect ratios are 200 and 300 nm, respectively.

they varied the distance between the gold nanospheres and CdTe nanowires and observed a shift in the photoluminescence emission that depended on the separation distance, an effect that may prove powerful in the fabrication of biosensors.

Recently, we reported on the electron dynamics in vertically aligned CdTe-Au core−shell nanorods as determined by femtosecond pump−probe techniques.[9] The transient bleach intensities, as well as the observed lifetimes, measured for the core−shell and for the CdTe standalone core structures revealed significant enhancements to the nonradiative relaxation rates of the hot electrons in the CdTe core upon exposure to the gold nanoshell in excitation regions at 530−550 and 750−780 nm. Theoretical calculations, based on the discrete dipole approximation (DDA), clearly showed that these two spectral regions correspond to energies that overlap with the localized surface plasmon oscillations of the gold nanoshell, a result that provided strong evidence that it is the "turning on" of the surface plasmon field that gives rise to the observed enhancements. Mechanisms by which these fields could increase the electronic relaxation were proposed. Most of these mechanisms involve radiative coupling between the surface plasmon electromagnetic field of the gold nanoshell and the moment of the electronic transition in the CdTe semiconductor. The increased radiative coupling (i.e., increased absorption rate) can either lead to the excited electron ionization or an increased excited electron density leading to Auger annihilation. In either case the lifetime of the excited electron decreases.

In order to assess these mechanisms one needs to examine the effect of changing the relative orientation of the surface plasmon field with respect to the direction of the electronic transition moment of CdTe. Such a study is possible only if all of the nanorods are oriented identically as is the case for substrate-based nanostructures where an epitaxial relationship with the underlying substrate facilitates the alignment. Then, through the tilting of the sample such that the polarization direction of the plasmon inducing exciting light goes from being normal to the long axis of the core−shell nanorod to one where it becomes progressively more parallel, it becomes possible to probe the anisotropy associated with the interactions between the gold nanoshell's plasmon fields and the electronic transition moment of CdTe. Here, we present such a study and observe a bandgap exciton lifetime dependence characterized by an enhancement to the relaxation rate as the polarization of the surface plasmon inducing light becomes increasingly parallel to the long axis of the core−shell nanorod. Simulations based on the discrete dipole approximation (DDA) are also carried out which demonstrate that at 770 nm the net polarization of the surface plasmon field is along the long axis of the core−shell nanorod when the polarization of the incident light is also along this direction. Because of the particular crystallographic alignment of the CdTe cores this same direction also corresponds to the transition moment of CdTe's excited states. It is thus concluded that the progressive enhancements to the relaxation rate as the core−shell nanorods are tilted arise from radiative coupling-type mechanisms that become progressively stronger as the gold nanoshell's plasmon fields and CdTe transition moments align.

Sample Preparation. A two-step process was used to fabricate the CdTe-Au core−shell nanorods. The first step relied on the vapor−liquid−solid (VLS) catalytic growth mode to produce substrate-based vertically aligned CdTe nanorods. The fabrication process is described in detail elsewhere.[10,11] The nanorods produced are single crystal in nature and share an epitaxial relationship with the underlying [0001] sapphire substrate. X-ray diffraction measurements indicate a wurtzite crystal structure instead of the zinc blende phase associated with the bulk material. Transmission electron microscopy shows excellent crystallinity with no evidence of the extensive stacking fault features associated with parasitic zinc blende phases. Unlike numerous other VLS-produced nanowires, the CdTe nanorods are completely isolated from one another at their base as the one-dimensional growth proceeds without the frequently observed slow, yet persistent, planar growth. In the second step, the CdTe nanorods, as well as the exposed substrate, are coated with a 15 nm thick gold shell using a sputter coater operating at room temperature. Figure 1 shows scanning electron microscope (SEM) images of the two samples used in this work. The first image (Figure 1a) shows core−shell nanorods where the aspect ratio is typically greater than three, while the second (Figure 1b) displays aspect ratios of less than two. The dissimilar aspect ratios are of significance to this work as they will give rise to distinctive plasmonic resonances. It is also important to note that a higher density of core−shell nanorods is found for the high aspect ratio sample.

Pump−Probe Experiments. The apparatus used in the femtosecond pump−probe experiments has been described

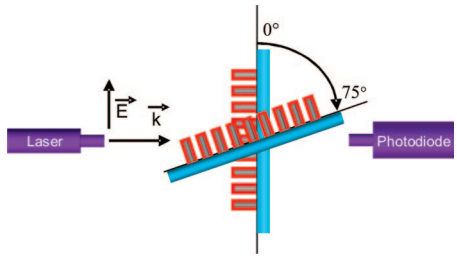

Figure 2. Schematic showing the experimental configuration used in the pump−probe experiments. The linearly polarized light of both the pump and probe pulses, having a propagation vector $\vec{k}$ and an electric field $\vec{E}$, is incident on the sample, which can be tilted from 0 to 75° away from the polarization direction of the light's electric field. CdTe, gold, and the sapphire substrate are shown in gray, red, and blue, respectively.

in detail elsewhere.[9] The technique allows for the excitation of hot electrons while monitoring their relaxation using a probe beam. The CdTe-Au core−shell nanorods were optically pumped with 400 nm pulses derived from frequency doubled 800 nm pulses (fwhm = 100 fs, energy = 1 mJ, repetition rate = 1 kHz). The probe beam is extracted from a white light continuum (λ = 400 to 1100 nm) generated by extracting a small percentage of the pump pulse and passing it through a sapphire plate. The pump and probe beam are then focused onto the sample to a spot size with a 250 μm diameter such that there is complete spatial overlap and variable temporal overlap. The experiment yields transient bleach intensities that provide a measure of the hot electron carrier dynamics within the core−shell nanorod. For the results presented here a probe wavelength of 770 nm is used exclusively so as to monitor the states just above the CdTe bandgap at 780 nm. With no bandgap emission observed and with the electrons excited to these states unable to relax significantly through intraband transitions, relaxation must proceed either through the electrons giving up their energy to phonons or to impurity scattering processes. The experimental configuration, shown schematically in Figure 2, allowed for the transient bleach intensities to be recorded as a function of angle. Note that it is only through sample tilting that the sides of the core−shell nanorods become illuminated with the incident pulses. Also of note is that both the pump and probe light are linearly polarized with their electric field vector along the length of the nanorod in the 90° tilt configuration. In this arrangement the electric field of the incident light has a component parallel, but not perpendicular to the optical plane of incidence. All measurements were performed at room temperature.

Bandgap Exciton Dynamics in CdTe-Au Core−Shell Nanorods. Figure 3a,b shows the temporal dependence of the normalized transient bleach intensity near the bandgap absorption (780 nm) as a function of tilt angle for the high and low aspect ratio CdTe-Au core−shell nanorods, respectively. Both samples show a marked increase in the relaxation rate as the nanorods are tilted, but with key differences. The high aspect ratio core−shell nanorods exhibit a steadily increasing relaxation rate as the sample is tilted with a response that saturates in the 60−75° range. The low aspect ratio nanorods do not exhibit this saturation in relaxation rate but instead show values which trend higher, albeit with an anomalously low value for the 60° tilt. At this angle, the relaxation rate is somewhat lower than that expected from the trend established by the remaining experimental data. All of these features can be clearly seen in Figure 4, which plots the decay rate constants extracted from transient bleach data. It is important to note that the observed effects are entirely dependent upon the presence of the gold shell as tilt measurements performed on just the CdTe cores showed no such dependencies.

Theoretical Response Derived from DDA Calculations. ***a. Tilt Dependence of the Optical Properties of CdTe-Au Core−Shell Nanorods.*** The tilt-dependent optical properties of the CdTe-Au core−shell nanorods were modeled using DDA simulations.[12−16] This finite-element computational method has proven widely applicable in predicting the optical response of plasmonic nanostructures of varying size, shape, and dielectric environment.[9,17−23] Here, approximately 10^5 dipoles were used to simulate a core−shell nanostructure comprised of a hemispherically capped CdTe nanorod with a gold shell covering all sides except for the base. Calculations were performed for nanostructures with aspect ratios of two and three and of similar dimensions to those used experimentally ($core_1$ = 184 × 74 nm, $shell_1$ = 15 nm, $core_2$ = 285 × 74 nm, $shell_2$ = 15 nm). The electric field enhancement and induced plasmon field polarization were calculated using codes provided by S. Li and G. C. Schatz (Northwestern University). Experimentally determined complex refractive indices for Au[24] and CdTe[25] were applied in an in vacuo environment. Interparticle near-field and exciton coupling interactions were assumed to be negligible at the microscopically observed interparticle distances.

The surface plasmon field causes an enhancement to the extinction cross-section of the gold nanostructures. Thus, the value of the plasmonic field at any wavelength determines the total extinction cross-section at this wavelength. For the present work, the wavelength of significance is 770 nm, which is the probe wavelength used to obtain the transient bleach intensity. Figure 5 shows a plot of the simulated extinction, absorption, and scattering cross-sections at 770 nm for the two aspect ratio core−shell nanorods as a function of the tilt angle. The low aspect ratio structure (Figure 5b) shows a gradual increase in both the absorption and scattering as the tilt angle is varied from 0 to 90°, which is in close agreement with previous simulations performed for both gold and silver nanorods.[26] In contrast, the high aspect ratio structure (Figure 5a) shows a concomitant increase in the scattering cross-section with increasing tilt angle but with an absorption and extinction that peaks near 50°.

b. The Surface Plasmon Field Enhancement and Polarization. Further insight is gained by extracting from the simulations the angular-dependent plasmon field enhancement and the induced polarization at the 770 nm probe wavelength for the two aspect ratio CdTe-Au core−shell nanorods. The four midpoint cross-sections, shown in Figure 6, display the plasmonic enhancement of the incident light's electric field intensity as a color contour map. Superimposed

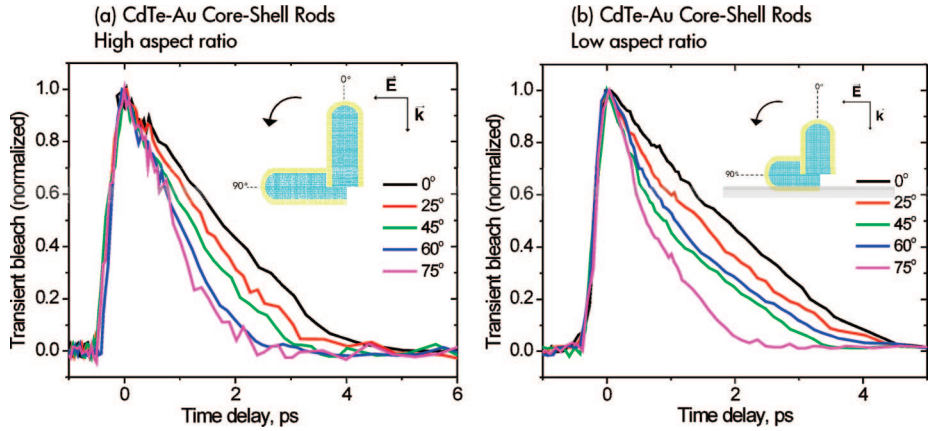

Figure 3. The temporal dependence of the transient bleach intensity recovery near the bandgap excitation of the CdTe semiconductor core (which provides a measure of the exciton's relaxation lifetime) as a function of tilt angle for CdTe-Au core−shell nanorods with aspect ratios (a) ≥3 and (b) ≤2. The data was taken using a 400 nm pump and a 770 nm probe wavelength. Note the response of the two structures differ at large tilt angles.

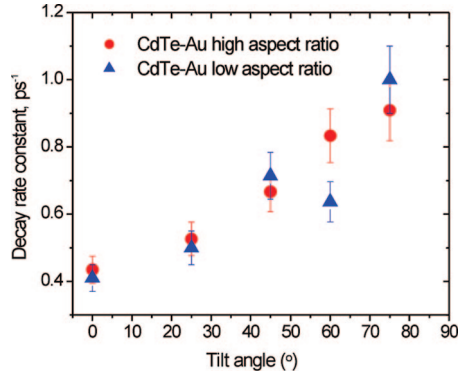

Figure 4. Plot of the exciton decay rate constant as a function of sample tilt for CdTe-Au core−shell nanorods with aspect ratios (a) ≥3 (red ●) and (b) ≤2 (blue ▲).

over this color map is a normalized grayscale map of the component of the induced plasmon field polarization parallel to the CdTe long axis. Figure 6a,b illustrates the field intensity and induced polarization for the 0° tilt (i.e., when the incident light's electric field is parallel to the short axis of the core−shell nanorod) for the low and high aspect ratio core−shell structures, respectively. For both of these cases, the color maps make it quite apparent that there is a significant plasmonic enhancement to the surrounding near-field at the 770 nm wavelength used. At the same time, the grayscale maps clearly display an anisotropic distribution in the induced plasmon field polarization with the upper portion of the cross-section showing negative polarization and the lower portion showing positive polarization. It should be noted, however, that the net plasmon field polarization along the long axis, obtained through an integration of both the dark and light regions, is zero. Figure 6c,d illustrates the same color and grayscale maps for the 90° tilt (i.e., when the incident light's electric field is parallel to the long axis of the core−shell nanorod) for the low and high aspect ratio core−shell structures, respectively. Once again, enhancements to the surrounding near-fields are observed at 770 nm. The induced plasmon field polarization for both cases, however, is markedly different from the 0° tilt configuration in that both the CdTe core and the gold shell each have a net polarization along the long axis that is clearly nonzero. Noteworthy, is the fact that the net plasmon field polarizations along the long axis for the CdTe core and the gold shell are opposite in sign.

Comparison of the Experimental and Theoretical Results. It is quite clear from the experimental results shown in Figure 4 that as one increases the core−shell nanorod tilt angle an enhancement of the bandgap exciton relaxation rate generally takes place. While this is clear for the high aspect ratio nanorods, there is a slight minimum at 60° for the low aspect ratio rods. While the overall trend is well described by the DDA simulations shown in Figure 5, the observation of this 60° minimum is not supported by these calculations and, as such, is unlikely to originate from direct surface plasmon field effects. The theoretical values obtained for the extinction (which are determined by the value of the field enhancement and, thus, the plasmonic field value) do indicate a smooth increase in the response with tilt angle for the low aspect ratio core−shell nanorods, but which saturates for angles greater than 55° (Figure 5b).

The anomalous 60° tilt result for the small core−shell rods is likely attributed to the angular dependence of the intensity of the light reflected off the thin gold film that coats the exposed substrate areas between the core−shell nanorods. Such a layer forms a mirrorlike surface that is able to reflect sufficient light onto the sides of the nanorods, leading to their additional excitation. The intensity of this reflected light can significantly impact the level of surface plasmon excitation and will vary with tilt angle as predicted by the Fresnel equation[27] with the electric field vector parallel to the plane of incidence. For the experimental configuration used here, the reflectance off this gold layer will gradually fall off as the sample is tilted, reaching a minimum at the Brewster angle, after which the reflectance rapidly rises. This rapid rise in the reflectance will, in turn, substantially increase the intensity of the light exciting the plasmon field of the core−shell nanorods. Thus, it is expected that any enhancements to the plasmon field arising from the reflected light off the gold thin film surface will be minimal at the Brewster

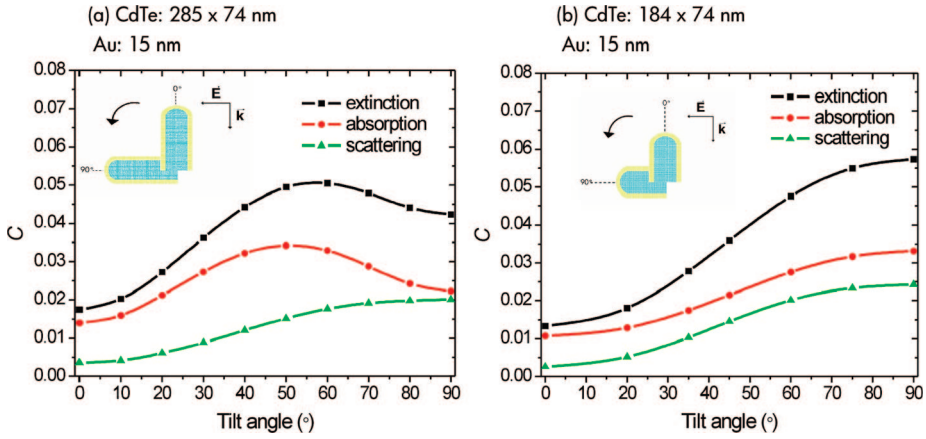

Figure 5. Plot of the DDA derived extinction (which monitors the plasmon field strength), absorption, and scattering cross-sections at 770 nm as a function of tilt for the core−shell nanorods with aspect ratios (a) ≥3 and (b) ≤2. Note that the angular dependence of the extinction increases monotonically for the low aspect ratio nanostructure while falling off at high tilt angles for the high aspect ratio structure.

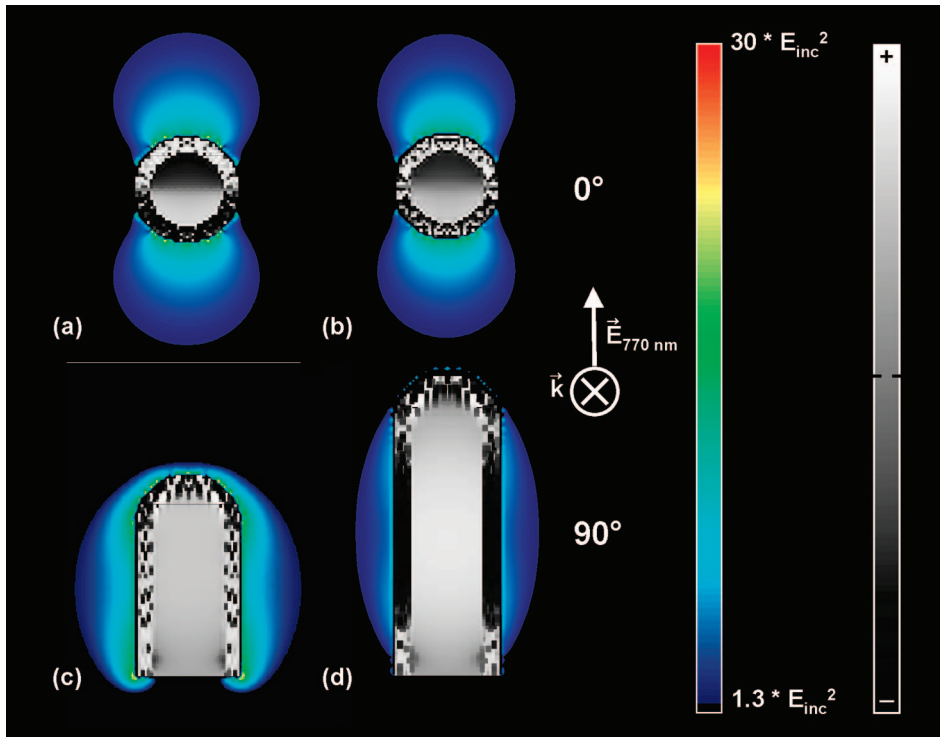

Figure 6. DDA simulation results depicting the enhancement (shown by the color contours) and induced polarization (shown by grayscale) of the plasmon field excited at 770 nm for CdTe-Au core−shell nanorods of the two aspect ratios used in the present study. (a,c) These panels show the midpoint cross-sections for a nanorod with an aspect ratio of two, while (b,d) are for an aspect ratio of three. The color contour maps show the surface plasmon field enhancement of the electric field intensity of the incident light when the electric field is along the short axis (i.e., 0° tilt) as is the case for panels a and b and along the long axis (i.e., 90° tilt) as is the case for panels c and d. The color bar scale denotes the enhancement factor of the incident electric field intensity. The grayscale maps, which are superimposed on the color maps, depict the normalized intensity plots of the induced plasmon field polarization in the core−shell nanorod for a direction parallel to the long axis of the nanorod. The grayscale bar denotes the degree of polarization where black and white correspond to opposing polarizations. The color contour plots clearly indicate the presence of a surface plasmon enhancement for both the 0 and 90° tilts. The grayscale plots show that a net plasmon field polarization is induced along the *c*-axis if the exciting light is polarized along the nanorod's long axis (i.e., 90° tilt), but not if it is along the short axis (i.e., 0° tilt), where the two polarizations of opposite sign cancel out one another.

angle, which for the gold-sapphire combination is near 60°.[27] While this provides an appealing explanation for the low relaxation rate observed at this angle, it does not explain why a similar feature is not observed for the high aspect ratio core−shell nanorods. This absence is likely explained by the fact that such an effect is to be diminished substantially, when compared to the low aspect ratio sample, due to the greater nanorod heights and density associated with the high aspect ratio sample (see Figure 1). This difference will lead to a smaller percentage of the surface that is mirrored and a much enhanced shadowing effect.

The Enhancement Mechanisms. While the experimental results indicate that the plasmon field has the strongest influence on the excited electron relaxation rates when its

forces are along the long axis of core−shell nanorod, the origin of this behavior has not as yet been addressed. One would expect that such a response could be facilitated by having the largest matrix elements of the perturbation responsible for the relaxation along this same axis. In this scenario, coupling between the plasmons and excitons would increase as the gold nanoshell's surface plasmon fields and the transition moment of the CdTe core come into alignment. In our previous publication,[9] we suggested several mechanisms that could account for the observed plasmon field effects on the relaxation rates of the semiconductor excitons. Some of them involve the enhancement of the radiative processes within the semiconductor that, in turn, increase the probability of either Auger or multiphoton ionization processes of the excited electrons within the semiconductor. Also suggested was a nonradiative process that involved energy transfer from the excited-state of the semiconductor to the gold nanoshell, a mechanism that excites the plasmon state of gold when in resonance with the excited-state of the semiconductor. All of these mechanisms involve coupling between the electromagnetic field of the plasmon and the transition moment of the semiconductor's excited-state when the frequencies of both excitations coincide (as was the case for the 530−550 and 750−780 nm surface plasmon resonances). It should first be recognized that the plasmon field is an electromagnetic field that resembles that of light. Also important to this discussion is the fact that the CdTe nanorods are epitaxially aligned with the *c*-axis of the wurtzite crystal structure aligned with the core−shell's long axis. Such a crystal structure will exhibit an ABAB...*c*-axis stacking sequence comprised of alternating layers of Cd^{2+} and Te^{2-} ions. The charge separation and thus the direction of the absorption transition moment in the CdTe nanorod is expected to be along the *c*-axis. The perturbation coupling interaction (H') between the plasmonic field ($\vec{E}_p$) and the exciton transition moment ($\vec{M}$) has the form

$$H' \approx \langle \vec{E}_p \vec{M} \rangle \quad (1)$$

This interaction thus dictates that the strongest perturbation of the plasmonic field on the exciton dynamic property should occur when the plasmon field direction is polarized parallel to the longitudinal *c*-axis direction of the core−shell nanorod. While it is observed experimentally that the effect on the lifetime increases with increasing tilt, the effect is not vanishing for the 0° tilt configuration as would be expected based on these arguments. Possible explanations for such behavior include (1) the slight misalignment of some of the nanorods with respect to the polarized electric field vector and/or (2) the fact that the polarization of plasmon field around the hemispherical nanorod top is mixed (as is clearly evident in Figure 6c,d).

Final Remarks and Conclusions. The results presented here bring to light a number of intriguing opportunities based on the anisotropic optical properties of aligned core−shell nanorods. Using the experimental configuration described here, it has been decisively demonstrated that exciton lifetimes can be modulated by more than 150%. It is also expected that such an effect would be further enhanced if there was greater overlap between the semiconductor bandgap energy and the maximum of the longitudinal plasmon mode whose extinction could be orders of magnitude larger. Such enhancements could be achieved through the optimization of the shell thickness or through the use of a lower bandgap semiconductor. These results also demonstrate that, while it was already well known that a number of factors such as the shape of the gold nanoshell, the excitation polarization, and the excitation wavelength all play an important role in determining the extent of the coupling, it is equally important to consider the crystallographic orientation of the semiconductor core relative to the long and short axes of the nanoshell.

The most important aspect of this work is the demonstrated ability to use plasmonic fields to tune the rates of electronic relaxation processes. Thus, there exists the potential to use these surface plasmon fields to control photochemical and photophysical processes in nature by changing their rate to a desired value. Plasmon fields have already been shown to influence the relaxation rates of hot electrons[9] in CdTe-Au core−shell nanorods at 550 nm and the rates of proton pump[28] and retinal photoisomerization[29] in bacteriorhodopsin photosynthesis. The present study demonstrates the possibility of tuning the rates of such processes, a capability that could prove quite effective in changing the functions involved or in elucidating the mechanisms of the processes taking place.

Acknowledgment. S.N. would like to acknowledge the financial support provided by the NSERC postdoctoral fellowship program. M.A.E. would like to thank the NSF-CHE (0554668). The McMaster University group would like to acknowledge the Canadian Institute for Advanced Research (CIFAR), the Natural Sciences and Engineering Research Council (NSERC), and the Ontario Research and Development Challenge Fund (ORDCF) under the auspices of the Ontario Photonics Consortium (OPC) for the funding provided and the Canadian Centre for Electron Microscopy (CCEM) for access to their facilities.

References

(1) Nie, S. M.; Emery, S. R. *Science* **1997**, *275*, 1102–1106.
(2) Huang, X. H.; El-Sayed, I. H.; Qian, W.; El-Sayed, M. A. *Nano Lett.* **2007**, *7*, 1591–1597.
(3) Schaadt, D. M.; Feng, B.; Yu, E. T. *Appl. Phys. Lett.* **2005**, *86*, 063106.
(4) Pillai, S.; Catchpole, K. R.; Trupke, T.; Green, M. A. *J. Appl. Phys.* **2007**, *101*, 093105.
(5) Sundararajan, S. P; Grady, N. K.; Mirin, N.; Halas, N. J. *Nano Lett.* **2008**, *8*, 624–630.
(6) Nakayama, K.; Tanabe, K.; Atwater, H. A. *Appl. Phys. Lett.* **2008**, *93*, 121904.
(7) Lee, J.; Govorov, A. O.; Dulka, J.; Kotov, N. A. *Nano Lett.* **2004**, *4*, 2323–2330.
(8) Lee, J.; Hernandez, P.; Lee, J; Govorov, A. O.; Kotov, N. A. *Nat. Mater.* **2007**, *6*, 291–295.
(9) Neretina, S.; Qian, W.; Dreaden, E.; El-Sayed, M. A.; Hughes, R. A.; Preston, J. S.; Mascher, P. *Nano Lett.* **2008**, *8*, 2410–2418.
(10) Neretina, S.; Hughes, R. A.; Britten, J. F.; Sochinskii, N. V.; Preston, J. S.; Mascher, P. *Nanotechnology* **2007**, *18*, 275301.
(11) Neretina, S.; Hughes, R. A.; Devenyi, G. A.; Sochinskii, N. V.; Preston, J. S.; Mascher, P. *Nanotechnology* **2008**, *19*, 185601.
(12) Draine, B. T. *Astrophys. J.* **1988**, *333*, 848–872.
(13) Draine, B. T.; Flatau, P. J. *J. Opt. Soc. Am. A* **1994**, *11*, 1491–1499.
(14) Draine, B. T.; Flatau, P. J. *DDSCAT 6.1 Scripps Institute of Oceanography*, University of California: San Diego, CA, 2005.

(15) Draine, B. T.; Goodman, J. *Astrophys. J.* **1993**, *405*, 685–697.
(16) Purcell, E. M.; Pennypacker, C. R. *Astrophys. J.* **1973**, *186*, 705–714.
(17) Hu, M.; Chen, J. Y.; Li, Z. Y.; Au, L.; Hartland, G. V.; Li, X. D.; Marquez, M.; Xia, Y. N. *Chem. Soc. Rev.* **2006**, *35*, 1084–1094.
(18) Jain, P. K.; Lee, K. S.; El-Sayed, I. H.; El-Sayed, M. A. *J. Phys. Chem. B* **2006**, *110*, 7238–7248.
(19) Kelly, K. L.; Coronado, E.; Zhao, L. L.; Schatz, G. C. *J. Phys. Chem. B* **2003**, *107*, 668–677.
(20) Lee, K. S.; El-Sayed, M. A. *J. Phys. Chem. B* **2005**, *109*, 20331–20338.
(21) Noguez, C. *J. Phys. Chem. C* **2007**, *111*, 3806–3819.
(22) Payne, E. K.; Shuford, K. L.; Park, S.; Schatz, G. C.; Mirkin, C. A. *J. Phys. Chem. B* **2006**, *110*, 2150–2154.
(23) Yang, W. H.; Schatz, G. C.; Vanduyne, R. P. *J. Chem. Phys.* **1995**, *103*, 869–875.
(24) Johnson, P. B.; Christy, R. W. *Phys. Rev. B* **1972**, *6*, 4370.
(25) *Handbook of optical constants of solids*; Palik, E. D., Ed.; Academic Press: New York, 1998; Vol. 1.
(26) Cortie, M. B.; Xu, X.; Ford, M. J. *Phys. Chem. Chem. Phys.* **2006**, *8*, 3520–3527.
(27) Hansen, W. *J. Opt. Soc. Am.* **1968**, *58*, 380–390.
(28) Biesso, A.; Qian, W.; El-Sayed, M. A. *J. Am. Chem. Soc*. **2009**, *131*, 2442−2443.
(29) Biesso, A.; Qian, W.; El-Sayed, M. A. *J. Am. Chem. Soc.* **2008**, *130*, 3258–3259.

NL900183M